COST EFFECTIVE GROWTH OF SILICON MONO INGOTS BY THE APPLICATION OF INCREASED PULL SPEED IN CZ-PULLER

F. Mosel[1], A.V. Denisov[1] , B. Klipp[1], R. Kunert[2], P. Dold[2]
[1] PVA Crystal Growing Sytems GmbH, Im Westpark 10-12, 35435 Wettenberg, Germany
[2] Fraunhofer-Center für Silizium-Photovoltaik CSP. Otto-Eißfeldt-Str.12, 06120 Halle (Saale), Germany
frank.mosel@pvatepla.com, phone: +49 64168690-125, fax: +49 64168690-822

ABSTRACT: The permanent demand on the improvement of solar cell efficiency and reduction of production costs has placed much focus on the multiple Cz-pulling techniques from a single crucible. PVA Crystal Growing Systems GmbH has developed a mobile recharge system for Czochralski pullers, the SiCharger MRS. This system and its potential was presented in detail at the 33rd EU PVSEC [1]. Another way to save costs while increasing productivity is a higher pull rate. In order to enable a higher pull speed at a stable crystal growth, the hot zone was investigated and optimized. The entire crystal growth arrangement was simulated with the commercial program package CGSim [2]. As a result, the pull rate could be significantly increased resulting in an appreciable saving of energy and process gas. In the next approach, an active crystal cooling system was implemented. This device consists of a water cooled container, which is placed a few centimeters above the phase boundary of the growing crystal, in order to increase the temperature gradient in the growing crystal close to its solidification interface. With this arrangement the heat transport through the crystal is improved. Crystals with 8 inch diameter were grown with a pull rate of 1.7 mm/min.

Keywords: Crystal Growth Rate, Simulation, Czochralski

1 INTRODUCTION

To meet the demand for an increase of the solar cell conversion efficiency and a reduction of the cost of the high quality monocrystalline substrate material, it is inevitable to optimize the whole value chain of crystalline silicon solar cells. A cost-intensive element in this chain is the conversion from the polycrystalline feedstock to the monocrystals by the Czochralski method. Economic analysis of the Czochralski technique identifies the crucible, furnace parts and the consumption of energy as the main cost drivers. To lower the production costs the application of multiple ingot growth from a single crucible is a powerful tool, as it was demonstrated by the authors [1]. Besides the cost savings an increase in productivity is also necessary. An increase of the pull rate is an effective tool to shorten the process time. Besides the increase of the pull speed and the cost efficiency, the material quality remains the key factor for the success in the PV market. That means that all economical improvements in the process conditions have to be justified by means of the quality of the grown ingots.

2 THEORY

2.1 Limitation of the growth rate in Cz-configuration

The physical rate limiting parameter for the growth of ingots in a Czochralski configuration is the dissipation of the latent heat of fusion of silicon at the interface crystal/melt by heat conduction through the growing ingot. The heat received from a crystal in contact with its melt can be determined as the heat of solidification plus the heat flux from the melt into the ingot. This situation can be written in a simple one dimensional model [3]:

$$(1) \quad \lambda_s \cdot \mathrm{A} \cdot \left(\frac{dT}{dx}\right)_S = \lambda_l \cdot \mathrm{A} \cdot \left(\frac{dT}{dx}\right)_l + \rho \cdot \mathrm{A} \cdot L \cdot v_p$$

In which λ is the thermal conductivity, A the area of the ingot, (dT/dx) is the axial temperature gradient, v_p is the constant growth velocity, ρ is the crystal density, L the latent heat of fusion and s,l are the subscripts for the solid and liquid phase. Assuming an isothermal melt i.e. $(dT/dx)_l = 0$ the maximum pull rate v_{pmax} can be estimated and related to the crystal radius r:

$$(2) \quad v_{p\max} = -\frac{\lambda_m}{\rho \cdot L}\left(\frac{dT}{dx}\right)_{x=0} = \frac{1}{\rho \cdot L}\sqrt{\left(\frac{2\sigma\varepsilon\lambda_m}{3 \cdot r} \cdot T_m^{\,5}\right)}$$

Here σ is the Stefan-Boltzmannn constant, ε is the surface emissivity, m is the subscript for melting temperature. For a detailed derivation of this equation see E. Billig [4].

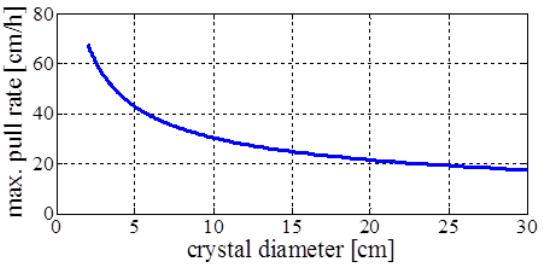

Figure 1: Max. crystal pull speed for silicon versus crystal diameter estimated by the model of E. Billig [4].

The model shows the inverse diameter square root dependency of the pull rate. It assumes the absence of thermal convection and a radiation from the crystal surface to the environment at zero Kelvin. The geometry of the hot zone especially in the hot growth region has a very complex geometry with different material parameters. S.N. Rea [5] has developed a thermal model which takes this situation to a certain degree into account. The calculated maximum pull rates show the same dependency of the crystal diameter as the model of Billig but with significant lower magnitudes. The curve of Rea is shown in Fig 2 together with the predicted maximum growth by models of Ciszek and Wilcox [6].
The interfacial temperature gradient is influenced by the thermal conditions at the crystal surface and not by its length. This holds for a crystal length which is twice its

diameter and a Biot number H > 0.15 [7]. This is the case for our growth conditions. The Biot number H for cylindrical surface (3) gives the ratio of the thermal

$$(3)\quad H = \frac{hr}{\lambda}$$

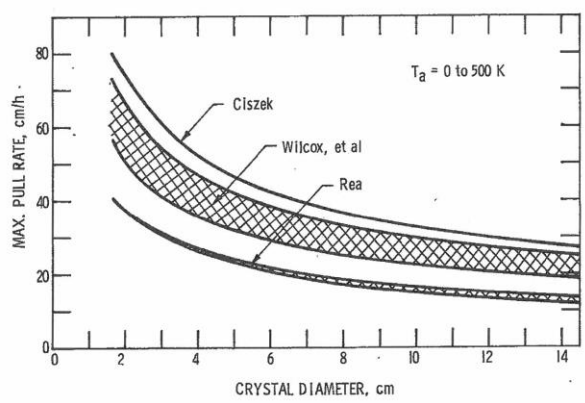

Figure 2: Silicon pull rates predicted by various models. The figure is reproduced from [6].

resistance within and at the surface of the ingot with r is the radius of the crystal, h is the convection heat transfer coefficient an λ is the thermal conductivity. In order to optimize all growth parameters especially the design of the hot zone including the inner heat shield, the application of numerical modeling of the Czochralski process is indispensable. The objective of the numerical simulation is to develop the growth conditions for a high pull rate which permits a stable crystal growth without the risk of losing the shape and crystallinity of the ingot.

2.2 Numerical simulation

The calculations were performed for 8 inch crystals in a 24 inch hot zone in a SC 24/26 crystal puller of PVA Crystal Growing Systems GmbH. In our development work we apply the CGSim software package from STR [2], which is especially developed for the Czochralski configuration. The following strategy was used for the simulation calculations. The standard hot zone was subjected to an extended analysis. The most important evaluation criteria are the deflection of the phase boundary (concavity), the radial temperature distribution on the melt surface and the axial temperature gradients in the center of the crystal and on its surface. The simulation calculations were carried out at a grown crystal length of 500 mm, since from this length no further change of the phase boundary shape is to be expected due to its Biot number. The deflection of the phase boundary should be as low as possible in order to ensure stable growth conditions. The knowledge of the curvature is also of importance for the distribution of intrinsic point defects, which is described by the well-known v/G criterion [8]. The radial temperature gradient in the melt at the crystal edge should be as high as possible and no supercooled areas with temperatures lower than the melt/crystal interface located close to the crystal should occur [9]. The axial temperature gradient in the crystal at the solid/liquid interface should be steep in order to enhance the dissipation of the latent heat in the crystal. The standard hot zone analyzed in this work is shown in Fig.3 on the left hand side. On the right hand side of Fig.3 the optimized design is shown. From the viewpoint of power reduction, the upper insulation was made more efficient. The inner radiation shield was completely reworked. Some of the important parameters of the geometry are indicated by arrows in fig.3.

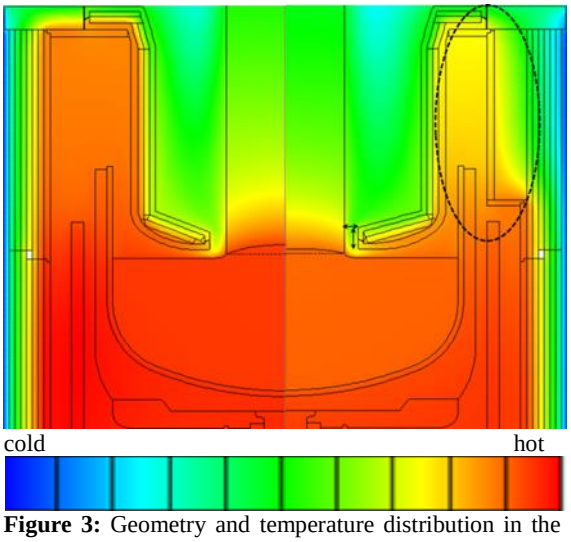

Figure 3: Geometry and temperature distribution in the standard (left hand side) and optimized (right hand side) hot zone.

Fig.5 shows a diagram which is based on the numerical simulations and the experience based on real crystal growth experiments. The interface curvature H is plotted versus the average pull speed in the body phase at a crystal length of 500 mm. 3 different regions are shown.in the diagram. In the stable growth region (green) the system is insensitive to changes in the average pull speed. This region is robust and suitable for industrial production. In the metastable growth region (yellow) all growth parameters have to be well tuned. Small changes can lead to unstable growth with loss of shape, i.e. spiral growth. In the unstable growth region (red) no regular crystal growth is possible.
In the graph the points connected by the lines represent individual results of the simulation calculations for the examined crystal growth arrangements (V1-V4). The open symbols in the graph represent experimental results. In cases V1 and V2 the deflections of the phase boundaries were determined by the LPS technique (see Fig.4).

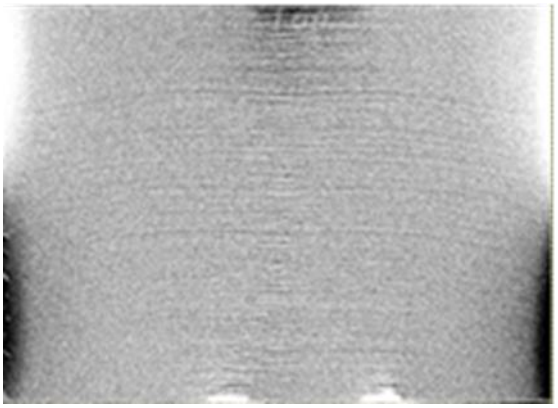

Figure 4: Growth striations revealed by the LPS technique [11] on a vertically sliced sample (205 mm x 250 mm), indicating the deflection of the growth interface.

The growth regions of the crystal growth configurations V3 and V4 have been determined experimentally by variation of the pull speed. The graph does not represent an analytical model but rather an empirically determined state diagram. In our crystal growth configuration the theoretical limit of the pull rate seems to lie in the range of 1.3 mm/min which can be achieved in principle by optimizing the inner heat shield and its integration in the standard hot zone (growth configuration V2).

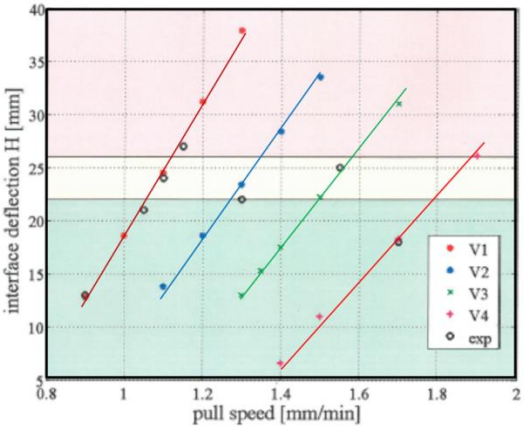

Figure 5: State diagram of the stable (green), metastable (yellow) and unstable (red) growth conditions. The main parameter deflection H of the interface shape is plotted versus the pull speed.

In order to achieve a further increase in the pull speed, an active crystal cooling system has been specifically integrated into this optimized hot zone. This active crystal cooling is a water-cooled container in form of a coil placed between the inner heat shield and the growing crystal. The crystal cooling coil configuration was first published by S.N. Rea in 1977 [6]. The principle of the arrangement is shown in Fig.6.

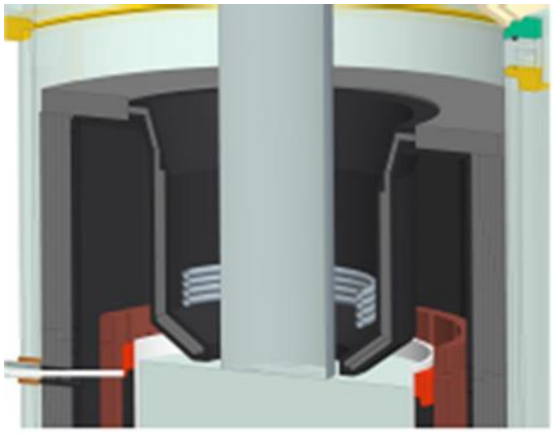

Figure 6: Arrangement of the active crystal cooling device in the hot zone.

The cooling coil is positioned in a certain distance to the melt. In this region the axial temperature gradient in the crystal at the phase boundary can be influenced effectively by the thermal conditions at the crystal surface. The geometry and its surface and especially the position of the cooling container with respect to the melt surface influence effectively the absorption capacity of the cooling device. The results of the numerical calculations are shown in Fig.7.

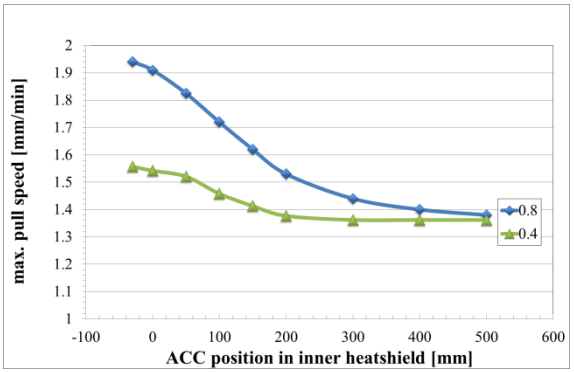

Figure 7: Maximum pull speed versus the distance of the cooling device to the melt surface for the emissivities 0.4 and 0.8. Position 0 represents the applied position of the lower edge of the cooling device in the growth configurations with a distance of 100 mm to the melt surface (-100).

Different geometries with different surface characteristics of the cooling devices have been tested and are still under investigation. Fig.8 shows two examples.

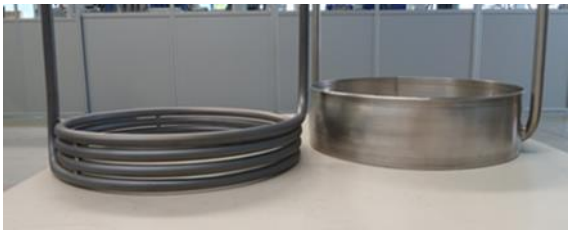

Figure 8: Cooling container with a spiral shape and a cylindrical shape.

It is well known that the temperature gradient at the crystallization interface, which is dependent on the crystal radius and the pull rate influence the distribution of intrinsic point defects. There is a critical ratio of the pull rate v_p to the temperature gradient G(r) of $v_p/G(r)$ = 0.134 mm^2/K min [10]. It was found that for a ratio more than the critical value v/G_{crit} vacancy aggregates develop and for a ratio lower than the critical value self-interstitial defects are predominant. At the critical ratio interstitials and vacancies annihilate each other and the crystal is free of dislocation loops and voids. Fig 9 shows the calculated values for the different crystal growth conditions. All applied growth conditions show a ratio v/G, which cause an intrinsic point defect distribution dominated by vacancies.

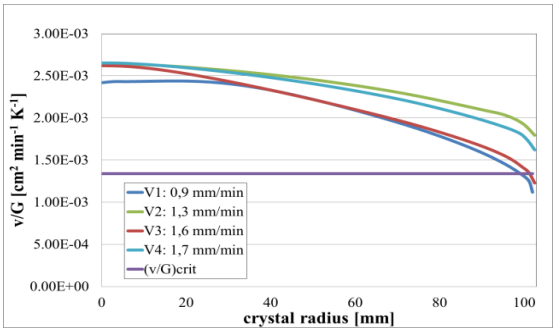

Figure 9: v/G ratio calculated for the applied crystal growth conditions (Tab.I).

3 CRYSTAL GROWTH

Several crystals have been grown in 4 different growth configurations V1 – V4, summarized in table 1. In growth configuration V1 and V2 no active cooling devices were applied, whereas in the growth configurations V3 and V4 two different cooling devices were tested. All growth configurations and their potential regarding the maximum pull speed are shown in the stability diagram in Fig.5.

growth configuration	hotzone	cooling device	emissivty	position of cooling device
V1	standard	no	-	-
V2	optimized	no	-	-
V3	optimized	cylinder	0.4	0
V4	optimized	spiral	0.6	0

Table I: Growth configurations with main parameters

3.1 Crystal Growth without active cooling

Several crystals have been grown under growth conditions without an active cooling device. The reference crystal in the standard hot zone (V1) was pulled with an average growth rate of 0.9 mm/min. The maximum average pull speed at which stable growth can be achieved in this configuration is 1.0 mm / min. At a pull speed of 1.15 mm/min spiral growth during the body phase was observed. From the reference crystal (V1) a vertical cut was prepared and the deflection of the solid/liquid interface was examined by the LPS-technique. The specimen was cut at a crystal length of 500 mm to make a comparison with numerical modeling possible. The concavity of the phase boundary of 13 mm, which was estimated from the photo is in good agreement with the calculated value of 12.5 mm. In the optimized hot zone (V2) a crystal was pulled with an average pull rate of 1.3 mm/min. It turned out that this pull speed already lies in the metastable range of the diagram (Fig.5). In a second growth run stable growth conditions were achieved by adjusting the distance of the inner heat shield to the melt surface. For these growth conditions the measured deflection of the interface was 23 mm compared to the calculated value of 22 mm. The good agreement confirms the results of the numerical simulation calculations.

3.2 Crystal Growth with active cooling

In order to achieve a higher pull speed, the axial gradient in the crystal must be increased according to equation 1. In the optimized hot zone of V2, which is the basis for the growth configuration V3 andV4, this was achieved by applying a water-cooled heat exchanger, hereinafter referred to as active crystal cooling. Such an arrangement was first described and experimentally investigated by S.N. Rea (6). The crystal cooling of Rea, however, led to an unstable growth process and thus this arrangement was not pursued further. Based on the work of S.N. Rea, the PVA Crystal Growing Systems GmbH developed an active crystal cooling system with different cooling devices. Examples are shown in Fig.8. The cooling device often referred to as cooling jacket in the literature is positioned between the inner heat shield and the growing crystal. The cooling element absorbs the radiant heat of the crystal and at the same time shields the crystal from the emitted heat radiation of the graphite inner heat shield. The development of the active crystal cooling system was carried out under strict safety considerations. The safety concept is discussed in detail in chapter 5. With the crystal growth configuration V3 a mean pull speed of 1.6 mm/min was achieved in the body phase from a length of approx. 100 mm after the transition from crown to body. With the crystal growth configuration of V4 a mean pull speed of 1.7 mm/min was possible. In this growth configuration too, the transition from the crown to the body lasted for some time. The process parameters in this area have to be optimized so that the transition to the fast pull speed is as short as possible.

3.3 Characterization of the grown ingots

The grown crystals V1, V2 and V4 were prepared for characterization as shown in Fig.10.

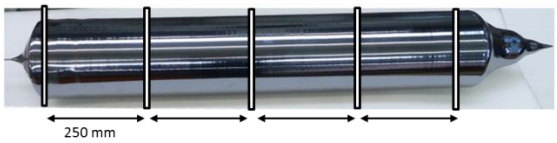

Figure 10: Position of the samples for characterization

5 slices were cut from the crystal at equal intervals and the contents of interstitial oxygen O_I and substitutional carbon C_S were investigated using FTIR. The conversion factor is 3.14×10^{17} cm^{-2} for O_I and 1.0×10^{17}cm^{-2} for C_S. The measurements on the wafer were performed 7 mm from the edge, half the radius and in the center. The measurement results are shown in Tab II. The samples are designated 1 to 5 from top to tail.

V1	sample 1	sample 2	sample 3	sample 4	sample 5	
center	10.8	9.1	8.2	7.5	6.5	x 10^{17} cm^{-3}
half radius	10.4	8.9	8.1	7.7	6.4	x 10^{17} cm^{-3}
edge	6.3	5.7	4.6	5.6	5.8	x 10^{17} cm^{-3}

V2	sample 1	sample 2	sample 3	sample 4	sample 5	
center	9.5	6.6	5.8	4.6	4.7	x 10^{17} cm^{-3}
half radius	9.2	6.6	5.6	4	4.3	x 10^{17} cm^{-3}
edge	3.6	3.2	2.3	1.6	3.6	x 10^{17} cm^{-3}

V4	sample 1	sample 2	sample 3	sample 4	sample 5	
center	10.8	6.1	6.1	8.6	9.7	x 10^{17} cm^{-3}
half radius	10.2	6	5.9	8.7	9.3	x 10^{17} cm^{-3}
edge	4.1	3.9	3.5	5.9	6.1	x 10^{17} cm^{-3}

Table II: O_I-concentration in the crystals V1, V2, V4. The C_S-concentration in 95% of all samples were below detection limit (<10^{16} cm^{-3})

The measurement results do not have any statistical certainty. However, it can be concluded that the high pull speed in the configurations V2 and V4 do not have a negative effect on the distribution of oxygen and carbon content.

4 ECONOMIC ANALYSIS OF THE HIGH PULL SPEED

The cost savings potentials of the different growth configurations are summarized in Tab.3. All data are based on the body phase only since this growth phase has defined boundary conditions (diameter, length). The other crystal growth phases are often different and not taken into account. The consumption of the heater energy is calculated from the effective power in the body phase. The consumptions of cooling water and gas correlate

with the pull rate in the body phase in the case of crystal growth configuration V1 and V2. In the case of crystal growth configuration V3 and V4 the consumption of the cooling water is enhanced due to the different cooling devices.

growth config.	mean pull speed. [mm/min]	time body phase [h]	Δ time body phase [%]
V1	0.9	20.5	0
V2	1.3	14.6	29
V3	1.6	12.05	41
V4	1.7	11.5	44

growth config.	Δ energy [%]	Δ argon [%]	Δ cooling water [%]
V1	0	0	0
V2	32	29	29
V3	41	41	39
V4	43	44	37

Table III: Measures of the productivity of the examined crystal growth configurations in the body phase. The Δ-data represent savings potentials referred to V1.

5 SAFETY CONSIDERATONS OF THE ACTIVE COOLING SYSTEM

5.1 Safety concept

The safety components in the control system of the puller detect faults in the cooling water circuit of the active cooling system and then switch off the water supply and the heater immediately. The water flow through the cooling circuit, the cooling water temperature at the outlet and the pressure inside the growth chamber are used as recognition and trigger criteria. The most important components are duplicated (redundant), so that if a sensor or actuator fails, the second one can take over and reset the machine to a safe state.

The greatest danger to man and machine is the uncontrolled discharge of water in the process chamber, which cannot be prevented, but the quantity of cooling water that may be released by the cooling device is kept low. Two series-connected, pneumatically actuated shut-off valves are located in the cooling water flow, two check valves connected in series in the return. This ensures that, in the worst case, only the quantity of water corresponding to the internal volume of the cooling device can enter into the process chamber, which is about 600 ml. When water enters the process chamber, a spontaneous pressure increase occurs. Two independent monitoring devices are used for overpressure detection. As soon as one of the two monitoring devices responds, the cooling water supply of the cooling device is stopped and the heating device is switched off. The flow rates and temperature of the cooling water of the crystal cooling are also monitored. If the temperature exceeds a fixed limit value or falls below the preset flow rate, the heating device is switched off. A short-term cooling water failure or pressure fluctuations are intercepted by a separate system for about 30 seconds. Before the start of each process the safety devices are automatically checked for perfect functionality.

The functionality of the shutdown due to a pressure increase in the process chamber was tested and confirmed under real crystal growth conditions.

5.2 Risk analysis

A risk analysis was carried out for the case where the cooling device, which is located a certain distance above the melt, has a water leak. Several reactions may occur:

A physical reaction where the transfer of water to vapour creates a steam explosion

A chemical reaction, where water reacts with the silicon metal and form hydrogen may lead in some situation to an oxyhydrogen reaction.

Physical reaction

When the water enters the process chamber, it is heated to 100° C. and evaporated. The evaporation enthalpy required for evaporation is provided by the melt surface and the surface of the internal heat shield. The following consideration was made for a water quantity of 1 liter. This corresponds to 55.6 mol of H_2O. In the puller with a free volume of about 1 m^3 this quantity would lead to a pressure of approx. 8 bar, if the mean gas temperature corresponds to the silicon melting temperature. Since the amount of water from the cooling device cannot be released instantaneously and a significantly lower gas temperature will adjust, a considerably lower pressure in the machine will be set for a short moment.

For the possibility of water entry with consequent steam formation and an increase of the internal pressure (steam explosion) several safety devices are installed in the puller, which react in succession at different pressures. If the pressure inside the growth chamber exceeds a value of 1.023 mbar the safety valve releases the overpressure.

Chemical reaction

(4) $Si + 2H_2O\ (gas) \rightarrow SiO_2 + 2H_2\ (gas)$

The water is poured on the surface of the silicon melt. The water is heated to 100°C and gas is formed. The water reacts with the melt at the surface and H_2 and SiO_2 are formed on the surface. The silicon oxide forms a continuous layer and a small amount of hydrogen is in the gas above the melt. The reaction according to equation (4) stops, while the water gas expands its volume.

The risk analysis was performed by the PVA Crystal Growing Systems GmbH together with SINTEF Materialer og kjemi, Norway.

5.3 Certificates

The set-up of the safety devices described in chapter 5.1 were checked and confirmed according to the guidelines EN ISO 13849-1:2008-12 by the German Technical Supervisory Board TÜV Hessen GmbH.

6 CONCLUSIONS

With an optimized design of the hot zone significantly higher pull speeds can be achieved. In this report an average growth rate of 1.3 mm/min in the body phase is shown. Further optimizations were investigated with numerical simulation calculations. The limit appears to be at 1.4 mm/min. With the use of an active crystal cooling system, an average pull speed of 1.7 mm/min was achieved. A further increase seems quite possible. The process parameters for such high growth rates still have to be optimized. The crystals grown with a high pull speed show good material characteristics with respect to the oxygen- and carbon concentrations compared to conventional pull rates. Statistical certainty is not possible within the scope of this work. The use of active crystal cooling promises a significant increase in

productivity combined with a high cost saving potential.

7 ACKNOWLEDGEMENTS

This work was supported by the German Ministry of Economy and Energy under contract number 0325883A.

8 REFERENCES

[1] F. Mosel, A.V. Denisov, B. Klipp, R. Sharma, R. Kunert, P. Dold, Proceedings 33rd European Photovoltaic Solar Energy Conference, München, Germany, (2016), 1064-1068
[2] CGSim package, STR Group,Ltd.
[3] J.C. Brice, J. Crystal Growth 2 (1968) 395-401
[4] E. Billig, Proc. Roy. Soc. (London) 229 (1955) 346-363
[5] S.N. Rea, J. Crystal Growth 54 (1981) 267-274
[6] S.N. Rea, Final Report, ERDA/JPL 954475 (April 1977)
[7] V.H. Kio, W. R. Wilcox, J. Crystal Growth 12 (1971) 191-194
[8] E. Dornberger, W.von Ammon, J. Virbulis, B. Hanna,. T. Sinno, J. Crystal Growth 230 (2001) 291-299
[9] V. Kalaev, A. Sattler, L. Kadinski, J. Crystal Growth 413 (2015) 12-16
[10] Fraunhofer-Center für Silizium-Photovoltaik CSP, Otto-Eißfeldt-Straße 12, 06120 Halle (Saale), Germany
[11] H.J. Schulze, A. Lüdge, H. Riemann, Electrochem. Soc. **143**, 4105 (1998)